Journal of
Synchrotron
Radiation

ISSN 1600-5775

Received 13 February 2014
Accepted 20 June 2014

Ptychography with multilayer Laue lenses

Adam Kubec,[a,b]* Stefan Braun,[b] Sven Niese,[c,d] Peter Krüger,[c] Jens Patommel,[e] Michael Hecker,[f] Andreas Leson[b] and Christian G. Schroer[e,g,h]

[a]Institute for Materials Science and Max Bergmann Center of Biomaterials, Technische Universität Dresden, 01062 Dresden, Germany, [b]Fraunhofer Institute for Material and Beam Technology, Winterbergstraße 28, 01277 Dresden, Germany, [c]Fraunhofer Institute for Ceramic Technologies and Systems, Winterbergstraße 28, 01277 Dresden, Germany, [d]Institute for Applied Physics and Sensors, BTU Cottbus-Senftenberg, 03046 Cottbus, Germany, [e]Institute of Structural Physics, Technische Universität Dresden, 01069 Dresden, Germany, [f]Center for Complex Analysis, GLOBALFOUNDRIES Dresden Module One LLC and Co KG, Wilschdorfer Landstraße 101, 01109 Dresden, Germany, [g]Deutsches Elektronen-Synchrotron DESY, Notkestraße 85, 22607 Hamburg, Germany, and [h]Fachbereich Physik, Universität Hamburg, Luruper Chaussee 149, 22761 Hamburg, Germany. *E-mail: adam.kubec@tu-dresden.de

Two different multilayer Laue lens designs were made with total deposition thicknesses of 48 µm and 53 µm, and focal lengths of 20.0 mm and 12.5 mm at 20.0 keV, respectively. From these two multilayer systems, several lenses were manufactured for one- and two-dimensional focusing. The latter is realised with a directly bonded assembly of two crossed lenses, that reduces the distance between the lenses in the beam direction to 30 µm and eliminates the necessity of producing different multilayer systems. Characterization of lens fabrication was performed using a laboratory X-ray microscope. Focusing properties have been investigated using ptychography.

Keywords: multilayer Laue lens; X-ray nanofocusing; ptychography; scanning X-ray microscopy.

© 2014 International Union of Crystallography

1. Introduction

X-ray microscopy is well suited to probe relatively thick specimens and thus enables virtually non-destructive testing of microscopic objects such as microchips (Schropp *et al.*, 2011) and other nanostructured materials. The resolution that can be achieved in X-ray microscopy is mainly limited by the available optics and thus improvements in focusing capabilities have direct impact on measurements.

A focus of 50 nm can be achieved with compound refractive lenses (Schroer *et al.*, 2005) and adiabatically focusing lenses aim for sub-20 nm resolutions (Schroer & Lengeler, 2005). Smallest hard X-ray beam sizes, *i.e.* 7 nm, have been achieved with multilayer mirror systems (Mimura *et al.*, 2009). Diffractive optics showed very promising results for hard X-rays providing a line focus with a width of 13 nm (Koyama *et al.*, 2011) and a focal spot size of 25 nm × 40 nm using crossed multilayer Laue lenses at 19.5 keV (Yan *et al.*, 2011). Theory predicts a focal size down to 5 nm with the current approach (Kang *et al.*, 2006). It has been discussed that the focus can be further reduced to less than 1 nm by geometrical improvements of the optics (Schroer, 2006; Yan *et al.*, 2007*b*).

For diffractive optics, the width of the individual zones has to obey the zone plate law (Attwood, 2000). The zones can be arranged in concentric rings on a membrane, or they can be deposited onto a planar or circular substrate. Such optics are known as Fresnel zone plates (FZP), multilayer Laue lenses (MLLs) and multilayer zone plates, respectively. MLLs have several technological advantages over FZPs, which lead to higher achievable resolutions and efficiencies. One of the limits for the resolution is the width of the outermost zone (Attwood, 2000; Born & Wolf, 1999). Thin film deposition techniques are able to produce structures of less than 1 nm (Wetzig & Schneider, 2003) while lithographic techniques are currently limited to zone widths of 10 nm or more (Chao *et al.*, 2010).

As the actual multilayer is deposited on a flat substrate with typical diameters of several centimeters, it is possible to prepare MLLs with virtually unlimited aspect ratios. The diffraction efficiency can be increased by the optimization of the section thickness of the lens according to the optimal aspect ratio for a specific application. This is especially important for hard X-rays as the relative phase shift of different materials decreases with higher energies. Even higher aspect ratios are necessary if volume diffraction is to be exploited. MLLs can be tilted to comply with a local Bragg condition increasing the local diffraction efficiency to up to 70%. The total diffraction efficiency of a wedged or curved MLL can exceed 60% (Kang *et al.*, 2006; Yan *et al.*, 2007*b*).

To obtain a point focusing device, either two MLLs have to be placed perpendicularly in series, or a wire core or a glass fiber can be used as a substrate to deposit the zones (multi-

Table 1
Multilayers and their characteristic values.

Focal lengths f, apertures A, as well as the diffraction-limited focal size δ_{dif} are given for the central region of the wafer at 20 keV.

Coating ID	Materials	f (mm)	Zones	A (μm)	δ_{dif} (nm)
PS6056	WSi_2/Si	20.0	50–2500	48	25.9
PS6359	WSi_2/Si	12.5	512–7000	53	14.4

layer zone plate) (Koyama *et al.*, 2012; Keskinbora *et al.*, 2013). Large MLL apertures used for X-ray experiments with a total deposition thickness of 43.5 μm have been demonstrated recently (Yan *et al.*, 2013).

Focusing characteristics of optics illuminated with a coherent light source can be obtained using ptychography. For MLLs this was previously demonstrated (Braun *et al.*, 2013; Huang *et al.*, 2013).

The lenses presented in this article offer a large aperture of the order of 50 μm. Such designs allow for long focal lengths and small focal diameters. This reduces significantly some of the experimental restrictions induced by short working distances. Two of such lenses have been combined to form a point focusing device. Those lenses can be used at lower energies with reasonable focal lengths as well. In particular, they can be applied in a laboratory X-ray microscope that operates mainly with Cu $K\alpha$ radiation (8.05 keV).

2. Fabrication of multilayer Laue lenses

A focus of 39 nm with an MLL fabricated from a coating with an illuminated aperture of 10 μm (Braun *et al.*, 2013) has previously been demonstrated. To obtain comparable focal sizes with longer focal lengths, lenses with larger apertures were produced in this study, as shown in Table 1. Alternating zones of amorphous WSi_2 and Si with thicknesses according to the zone plate law were deposited using magnetron sputter deposition on a commercially available 150 mm single-crystalline silicon wafer. The process was started with the outermost zones to ensure lowest interfacial roughness for the thinnest layers. The deposition took 53 h for the deposition PS6056 and 83 h for PS6359. The wafers were subsequently annealed to reduce residual stress.

The actual lens was produced similarly to an H-bar lamella for transmission electron microscopy (Giannuzzi & Stevie, 1999). A bar with a thickness t_b of less than 100 μm and a length of several millimeters was cut from the wafer. Subsequently, a w = 80 μm-wide part of the multilayer stack was thinned with focused ion beam (FIB) milling to the desired section thickness t. To obtain a two-dimensionally focusing device, two of such bars are then glue-bonded perpendicularly onto each other (Fig. 1). The depth of focus is shorter than the physical distance between the lens elements. To compensate for this, the deposition process was modified to obtain a small radial thickness gradient. Lenses with matched focal lengths were obtained from different positions on the substrate.

3. MLL characterization with a laboratory X-ray microscope

A first characterization of the lenses is carried out in an Xradia NanoXCT-100 laboratory X-ray microscope (Tkachuk *et al.*, 2006) in order to obtain information about the quality of the coating and the thinning process. Radiographs of each MLL were acquired using the built-in Fresnel zone plate with a field of view of 65 μm × 65 μm, and defects like embedded particles and layer delaminations were directly observed.

Locally, the MLL acts as a diffraction grating with constant d-spacings. A reduction of the intensity is therefore expected in transmission, when the grating complies with the respective Bragg condition. Globally, the zone width is increasing in the normal direction of the multilayer stack. Thus, diffraction only occurs within a specific region of the lens according to the respective tilt angle of the MLL and a corresponding straight extinction pattern along the width of the lens is observed. Any deviation such as curved patterns are an indication for an elastically deformed or otherwise flawed lens element. The deformation may be caused by residual stress resulting from the multilayer deposition or FIB processing.

Results of measurements with synchrotron radiation using the high-resolution X-ray camera are in agreement with observations in the laboratory X-ray microscope, although the latter one provides a hollow cone illumination rather than an almost parallel X-ray beam. Fig. 2 shows radiographs of similar deformed lenses for both microscopes. The initial characterization at the laboratory microscope is able to monitor optimizations in the fabrication process. A final inspection of each lens is made prior to synchrotron experiments.

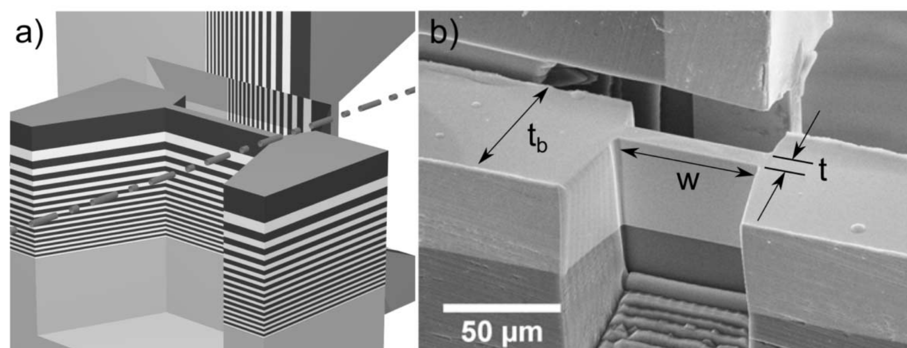

Figure 1
(*a*) Scheme and (*b*) SEM image of crossed MLLs. t is the section thickness, t_b the thickness of the bar, and w the width of the lens element.

4. MLL characterization at the synchrotron beamline P06 at PETRA III

Experiments using synchrotron radiation were carried out at the nanoprobe beamline P06 at PETRA III in Hamburg, Germany (Schroer *et al.*, 2010). The most important components

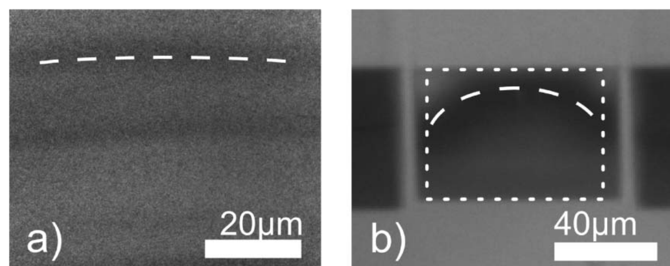

Figure 2
(*a*) Absorption contrast image of the MLL in the Xradia NanoXCT-100. From the curved extinction pattern a bending of the lens element can be concluded. (*b*) The same type of bending observed at the PETRA III beamline P06. The field of view of (*a*) is indicated as a dashed rectangle.

of this beamline are discussed in the following. Slits are used to limit the size of the beam to the size of the aperture of the lenses. Two sets of stages provide ten degrees of freedom in translation and rotation to individually align a horizontally and a vertically focusing lens. A pinhole is used as order-sorting aperture. A fluorescence detector is placed sideways from the sample mount. Either a high-resolution X-ray camera, an optical microscope, a PIN-diode or an X-ray pixel detector can be placed downstream of the object. Two basic set-ups are used for the presented experiments to obtain a point focus. An MLL was arranged in a crossed geometry with a nanofocusing refractive X-ray lens (NFL) (Schroer *et al.*, 2004). For this combination it is necessary to align both lenses individually according to their individual strategies as well as relatively to each other similar to other combinations of two one-dimensionally focusing optics. The alignment procedure for an NFL is described by Patommel (2010). The etching depth of an NFL structure is approximately 50 μm and this depth is the limiting factor for the maximum usable MLL aperture in this particular combination. The focusing characteristics of NFLs are well known and easy to interpret. This allows easier characterization of the MLL and imposes less restrictive requirements on the relative angular alignment of the lenses.

Pairs of already crossed MLLs need only one set of the available stages having two degrees of freedom each in rotation and translation, respectively.

To set up a pair of individual lenses, they have to be aligned separately in the beam using the high-resolution X-ray camera. Coarse positioning in the beam direction is performed during the mounting of the lenses. For MLL alignment the position of the camera is about twice the focal length downstream of the lens. The MLL is tilted at a range of angles at which the transmission through the lens in zeroth order is significantly reduced and the intensity of the first focusing order becomes significantly pronounced. The rocking angle that corresponds to the maximum intensity in the first focusing diffraction order is chosen. Subsequently, the apertures of MLL and NFL are placed behind each other. Slits upstream of the lenses are used to illuminate exclusively the aperture of the lenses or selected parts.

To block all orders except the first focusing order, the maximum size of the pinhole is determined by the distance of the zeroth- and higher-order beams as shown in Fig. 3(*a*). It is positioned downstream from the position where the zeroth- and first-focusing-order beams separate and its size is limited by the distance to higher orders.

The effective working distance arises from the distance pinhole–focal-plane of the lenses. In order to find the optimal position of the pinhole, the intensity on the PIN-diode is measured as a function of the position of the pinhole perpendicular to the beam in the respective focusing direction of each lens. An exemplary measurement is shown in Fig. 3(*b*), which roughly corresponds to the set-up and the pinhole positions in Fig. 3(*a*). The separate peaks in intensity represent the different diffraction orders of the lens. The measurement took place with the pinhole at a plane, where the distance between zeroth and first focusing order is larger than the pinhole diameter. The optimal position is in the center of the first-order plateau.

The focusing characteristics of NFLs are well known. A combination of NFL and MLL clearly reveals differences with respect to alignment and focusing. Figs. 4(*a*), 4(*b*) and 4(*c*) show images of the high-resolution X-ray camera, after both apertures had been matched, and position and aperture of the slits were adapted, respectively.

Knife-edge scans are conducted to measure the positions of the focal planes in the beam direction. A corner of a rectangular silicon substrate coated with an 80 nm gold layer is used as a test pattern. Clear edges were made by FIB milling. Using the fluorescence detector, the intensity of the Au-*L* signal is recorded while the edge is moved perpendicularly to the beam. This is repeated at different positions along the beam direction. The focus is located near the position with the steepest gradient of the fluorescence signal. With knife-edge

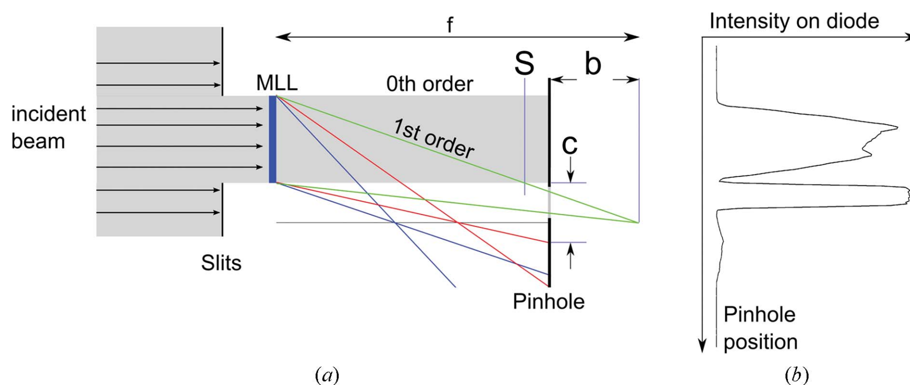

Figure 3
(*a*) Scheme of the focusing order distribution of a single MLL. *S* is the plane where zeroth- and first-order separate, *b* is the working distance of the set-up, *c* the maximum size of the pinhole at the given position and *f* is the focal length of the lens. (*b*) Measured intensity with the PIN-diode moving the pinhole through the different orders. The graph represents a set-up where the distance of zeroth- and first-focusing-order is of the order of the size of the pinhole.

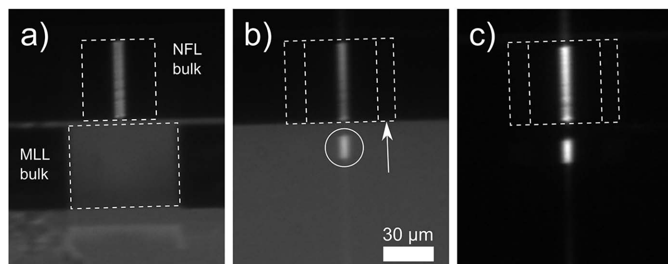

Figure 4
(*a*) Transmission image of an aligned nanofocusing refractive lens and an MLL lamella. The X-ray camera is placed downstream of the focal planes of the lenses. The dashed rectangles indicate the approximate apertures of the respective lenses. The NFL is located above the MLL. The focused beam appears inside the rectangle in the case of the NFL. For the MLL the focused beam is observed at an off-axis position below its aperture. (*b*) Consecutively arranged NFL and MLL. The arrow indicates the MLL movement relative to (*a*). The bright spot highlighted by the circle is the first-focusing-order diffracted beam from the MLL, which also passed the NFL. (*c*) The position of the lenses remains unchanged, while the slits have been positioned to limit the incident beam to the apertures of both lenses. The first-order diffracted beam is now separated from the flat-field.

measurements the relative position of both foci is determined and subsequently adjusted to an accuracy of better than 100 µm. Fine adjustment down to accuracies better than the depth of focus is performed using ptychography.

Ptychography, a coherent diffraction microscopy technique (Thibault *et al.*, 2008), allows beam and sample characterization with coherent radiation sources. The sample is scanned two-dimensionally with a coherent beam and the far-field diffraction pattern is recorded at each position. An overlap of the illumination of adjacent scan points is necessary (Bunk *et al.*, 2008). Fluorescence data are recorded simultaneously as complementary information. It is possible to reconstruct the complex transmission function of the sample and the complex wavefield of the illuminating beam allowing for a full characterization of beam and specimen (Schropp *et al.*, 2011; Hönig *et al.*, 2011). The results of the ptychographic reconstruction allow the calculation of a complete caustic of the optics set-up by numerical propagation.

5. Results

In a crossed-lens set-up of MLL and NFL, a lens made from PS6056 with a section thickness of t = 10.5 µm was characterized. The caustic of the beam in the focusing direction of the MLL and the profile of the beam in the focal plane are shown in Fig. 5. The full width at half-maximum of the focus was determined to be 42 nm. The beam profile shows significant side lobes. It is evident that the measured caustics behave similarly to the calculated caustics of Yan *et al.* (2007*a*). Calculations have shown that this is resulting from a drift of the deposition rate of approximately 0.75% during the fabrication.

Three set-ups of pairs of crossed MLLs were evaluated. Crossed lenses from the deposition PS6056 were made with section thicknesses of approximately t = 4.0 µm and t = 10.5 µm corresponding to the optimal phase shift at photon

Figure 5
Calculated caustic based on the ptychography measurements for a lens made from the deposition PS6056. Side lobes in the intensity profile are evident. The vertical axis represents the focusing direction while the horizontal axis represents the propagation direction.

energies of 8 keV and 20 keV, respectively. In addition, a pair of crossed MLLs was obtained from PS6359 with a section thickness of approximately t = 10.5 µm. A Siemens star test pattern (X30-30-1; Xradia Inc.) was used as the sample to demonstrate the focusing capabilities. Sizes and shapes of the focal spot were determined by the illumination that was gained from the ptychographic reconstruction. For the crossed MLLs of PS6056 with t = 10.5 µm, a beam size of 42 nm × 49 nm was determined. The amplitude of the reconstructed wavefield shows a distribution of the intensity concentrated in the central focus. The side lobes are located mostly diagonally to the axes along focusing directions. This is a result of the superposition of the diffraction effects of the individual lenses and an imperfect perpendicular alignment (Fig. 6*a*). The flux passing the slits without lens and pinhole in place was compared with the flux on the PIN-diode with lenses and pinhole in place. The latter measured flux was determined to be 5.22×10^7 photons s^{-1}. This is 11.5% of the flux with only the slits in place, which is considered to be the efficiency of the lens. The efficiency of the individual lenses cannot be determined using this method; however, the efficiency of a single lens can be estimated by the square root of the total efficiency, *i.e.* 33.9%, assuming similar efficiencies for both optics.

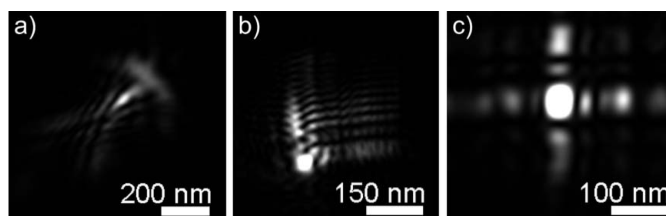

Figure 6
Intensity of the reconstructed wavefields of lenses from the deposition PS6056 with a lamella thickness of (*a*) 10.5 µm and (*b*) 4.0 µm and the deposition PS6359 with a lamella thickness of (*c*) 10.5 µm in their respective focal planes. Lenses from PS6056 with a reduced lamella thickness show less volume diffraction effects and the individual lenses show their respective side lobes caused by the rate drift in the deposition process. For the PS6359 version of the lens the side lobes are mainly located on the focusing axes of the lenses and their intensity and shape improved compared with the previous ones. The sizes of the central peaks are 40 nm × 44 nm, 42 nm × 47 nm and 39 nm × 49 nm for (*a*), (*b*) and (*c*), respectively.

In Fig. 6(*b*) the amplitude for a pair of crossed MLLs from the same deposition with a section thickness of 4.0 µm is shown. The side lobes are mainly located on the vertical and horizontal axes. Their superposition is found in the upper right corner. This is a result of a better perpendicular alignment compared with the set-up in Fig. 6(*a*). The side lobes show comparable shape to a lens produced from the same deposition and used in a crossed set-up together with a matching NFL as seen in Fig. 5.

For the deposition PS6359, a drift correction was implemented into the deposition process. It corrects the deviation of the deposition rate during the process time with respect to the initial value. A linear drift as a function of the total deposition thickness was assumed based on measurements with the earlier deposition. The result shows a reduction of the intensity of the side lobes in the beam profile in the immediate neighborhood of the main peak (Fig. 6*c*). The size of the central peak is 39 nm × 49 nm. For the crossed lenses, the distance between the individual focal planes is of the order of 20 µm.

Fig. 7 shows the reconstructed phase images of the sample. It is evident that the gold walls down to 30 nm-wide found in the innermost part seem to suffer in contrast between every other structure. This result was reproducible. It is assumed that the high-aspect-ratio gold patterns were degraded and some of the adjacent bars collapsed due to plastic deformation.

To demonstrate the capability of MLLs to handle sample measurements in the hard X-ray regime, a semiconductor test sample from GLOBALFOUNDRIES was used. A ptychographic measurement was performed and the corresponding fluorescence intensities were recorded. Fig. 8 shows the respective results of the reconstruction and the fluorescence maps for the tantalum and copper channels. In Fig. 9 the same area measured with the NanoXCT-100 is shown. Ptychography shows a significant improvement in resolution compared with the fluorescence data and full-field imaging.

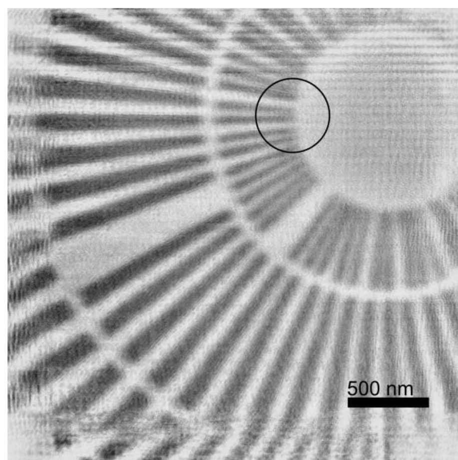

Figure 7
Reconstruction of the object phase of the Siemens star probed with a focus of a pair of crossed MLLs. The image represents an area of 2.8 µm × 2.8 µm. The circle indicates an example of neighboring collapsed gold structures.

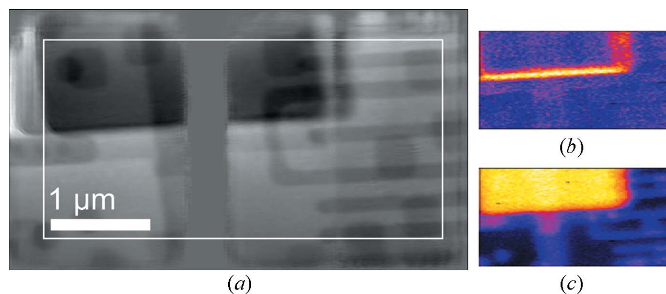

Figure 8
(*a*) Ptychographic reconstruction of the GLOBALFOUNDRIES integrated circuit sample and fluorescence maps of the (*b*) tantalum and (*c*) copper channels. Due to a malfunction of the trigger system about one-third of the far-field diffraction images could not be used for ptychographic reconstruction. The white rectangle in the reconstruction indicates the scanned region.

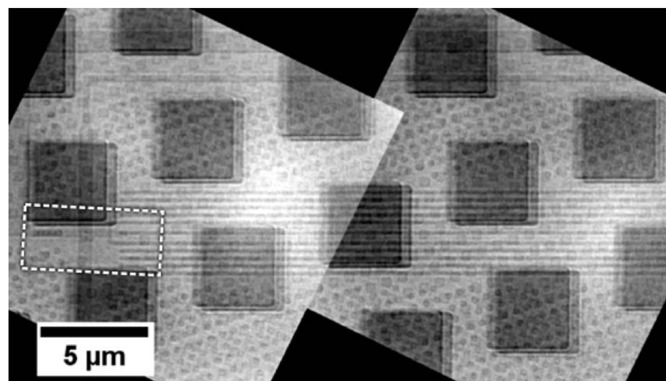

Figure 9
Stitched and rotated radiographs of the region of interest of the thinned chip acquired with the X-ray microscope Xradia NanoXCT-100 with the high-resolution 40× FZP. Copper circuit lines of the actual wiring layout are overlaid by some larger copper tiles. The area being investigated with ptychography is indicated with the dashed rectangle.

6. Conclusion

MLL depositions with total thicknesses of the order of 50 µm consisting of more than 6400 layers with individual zone widths down to 5 nm, and focal lengths of 12.5 mm and 20.0 mm at 20 keV photon energy were produced.

Experiments were performed with a combination of one MLL with a nanofocusing refractive lens as well as with pairs of crossed MLLs. The lenses for the latter combination had been pre-aligned using glue-bonding and they were attached to a single mount. This reduces the number of degrees of freedom necessary for alignment at the beamline to only four. A significant reduction of time needed for the alignment was experienced compared with set-ups with individual holders. A laboratory X-ray microscope was used for initial characterization of the MLLs. The relative alignment of the crossed lenses was tested, and artifacts related to the preparation or residual stresses could be observed. Successful ptychographic measurements were performed with all mentioned combinations of lenses, allowing for the characterization of beam properties and analysis of the samples. For the crossed MLLs, a beam size of below 50 nm full width at half-maximum was

achieved. A crossed lens set-up of the PS6056 version of the deposition showed a total efficiency for the lens set-up of 11.5% resulting in an estimated efficiency for the individual lenses of 33.9%. The caustic shows side lobes in the beam profile caused by a rate drift during the multilayer deposition. This experience was used to improve the subsequent deposition PS6359, where the intensity of the side lobes was reduced significantly. A more precise characterization of the drift characteristics, reduction of the accumulated stress, more precise alignment of the lenses, and the increase of the effective aperture remain as further challenges for future lenses.

This work is partly funded by the projects ENano and CoolAnalytics. The project ENano (100087859) is funded by the European Social Fund and the Free State of Saxony. The project CoolAnalytics is part of the Leading-Edge Cluster 'Cool Silicon', which is sponsored by the Federal Ministry of Education and Research (BMBF) within the scope of its Leading-Edge Cluster Competition. Portions of this research were carried out at the light source PETRA III at DESY, a member of the Helmholtz Association (HGF). We would like to thank Ulrike Bösenberg, Gerd Wellenreuther and Gerald Falkenberg for assistance in using beamline P06.

References

Attwood, D. T. (2000). *Soft X-rays and Extreme Ultraviolet Radiation: Principles and Applications.* Cambridge University Press.

Born, M. & Wolf, E. (1999). *Principles of Optics: Electromagnetic Theory of Propagation, Interference and Diffraction of Light*, CUP Archive.

Braun, S., Kubec, A., Menzel, M., Niese, S., Krüger, P., Seiboth, F., Patommel, J. & Schroer, C. (2013). *J. Phys. Conf. Ser.* **425**, 052019.

Bunk, O., Dierolf, M., Kynde, S., Johnson, I., Marti, O. & Pfeiffer, F. (2008). *Ultramicroscopy*, **108**, 481–487.

Chao, W., Kim, J., Rekawa, S., Fischer, P. & Anderson, E. H. (2010). *Opt Express*, **17**, 17669–17677.

Giannuzzi, L. & Stevie, F. (1999). *Micron*, **30**, 197–204.

Hönig, S., Hoppe, R., Patommel, J., Schropp, A., Stephan, S., Sebastian, S., Burghammer, M. & Schroer, C. G. (2011). *Opt. Express*, **19**, 16324–16329.

Huang, X., Yan, H., Nazaretski, E., Conley, R., Bouet, N., Zhou, J., Lauer, K., Li, L., Eom, D., Legnini, D., Harder, R., Robinson, I. K. & Chu, Y. S. (2013). *Sci. Rep.* **3**, 3562.

Kang, H., Maser, J., Stephenson, G., Liu, C., Conley, R., Macrander, A. & Vogt, S. (2006). *Phys. Rev. Lett.* **96**, 127401.

Keskinbora, K., Robisch, A.-L., Mayer, M., Grévent, C., Szeghalmi, A. V., Knez, M., Weigand, M., Snigireva, I., Snigirev, A., Salditt, T. & Schütz, G. (2013). *Proc. SPIE*, **8851**, 885119.

Koyama, T., Takano, H., Konishi, S., Tsuji, T., Takenaka, H., Ichimaru, S., Ohchi, T. & Kagoshima, Y. (2012). *Rev. Sci. Instrum.* **83**, 013705.

Koyama, T., Takenaka, H., Ichimaru, S., Ohchi, T., Tsuji, T., Takano, H. & Kagoshima, Y. (2011). *AIP Conf. Proc.* **1365**, 24.

Mimura, H., Handa, S., Kimura, T., Yumoto, H., Yamakawa, D., Yokoyama, H., Matsuyama, S., Inagaki, K., Yamamura, K., Sano, Y., Tamasaku, K., Nishino, Y., Yabashi, M., Ishikawa, T. & Yamauchi, K. (2009). *Nat. Phys.* **6**, 122–125.

Patommel, J. (2010). PhD thesis, Technische Universität Dresden, Germany.

Schroer, C. G. (2006). *Phys. Rev. B*, **74**, 033405.

Schroer, C. G., Boye, P., Feldkamp, J. M., Patommel, J., Samberg, D., Schropp, A., Schwab, A., Stephan, S., Falkenberg, G., Wellenreuther, G. & Reimers, N. (2010). *Nucl. Instrum. Methods Phys. Res. A*, **616**, 93–97.

Schroer, C. G., Kuhlmann, M., Kurapova, O., Hunger, U., Gunzler, T. F., Feste, S., Lengeler, B., Ziegler, S., Drakopoulos, M., Burghammer, M., Riekel, C., Snigirev, A. & Snigireva, I. (2004). *Proc. SPIE*, **5539**, 10–19.

Schroer, C., Kurapova, O., Patommel, J., Boye, P., Feldkamp, J., Lengeler, B., Burghammer, M., Riekel, C., Vincze, L., Van der Hart, A. & Küchler, M. (2005). *Appl. Phys. Lett.* **87**, 124103.

Schroer, C. G. & Lengeler, B. (2005). *Phys. Rev. Lett.* **94**, 054802.

Schropp, A., Boye, P., Goldschmidt, A., Hönig, S., Hoppe, R., Patommel, J., Rakete, C., Samberg, D., Stephan, S., Schöder, S., Burghammer, M. & Schroer, C. G. (2011). *J. Microsc.* **241**, 9–12.

Thibault, P., Dierolf, M., Menzel, A., Bunk, O., David, C. & Pfeiffer, F. (2008). *Science*, **321**, 379–382.

Tkachuk, A., Feser, M., Cui, H., Duewer, F., Chang, H. & Yun, W. (2006). *Proc. SPIE*, **6318**, 63181D.

Wetzig, K. & Schneider, C. M. (2003). *Metal-Based Thin Films for Electronics.* Wiley Online Library.

Yan, H., Chu, Y. S., Maser, J., Nazaretski, E., Kim, J., Kang, H. C., Lombardo, J. J. & Chiu, W. K. (2013). *Sci. Rep.* **3**, 1307.

Yan, H., Kang, H., Maser, J., Macrander, A., Kewish, C., Liu, C., Conley, R. & Stephenson, G. (2007*a*). *Nucl. Instrum. Methods Phys. Res. A*, **582**, 126–128.

Yan, H., Maser, J., Macrander, A., Shen, Q., Vogt, S., Stephenson, G. B. & Kang, H. C. (2007*b*). *Phys. Rev. B*, **76**, 115438.

Yan, H., Rose, V., Shu, D., Lima, E., Kang, H. C., Conley, R., Liu, C., Jahedi, N., Macrander, A. T., Stephenson, G. B., Holt, M., Chu, Y. S., Lu, M. & Maser, J. (2011). *Opt. Express*, **19**, 15069–15076.